

Molecular Rovibrational Spectroscopy with Undetected Photons via Single-Photon Interferometry

Sun Kyung Lee,^{1,†} Tai Hyun Yoon,^{1,2,*} and Minhaeng Cho,^{1,3,†}

¹*Center for Molecular Spectroscopy and Dynamics, Institute for Basic Science (IBS), Seoul 02841, Republic of Korea*

²*Department of Physics, Korea University, Seoul 02841, Republic of Korea*

³*Department of Chemistry, Korea University, Seoul 02841, Republic of Korea*



(Received 6 March 2020; revised 22 May 2020; accepted 8 June 2020; published 15 July 2020)

Interferometric spectroscopy with undetected photons (ISUP) utilizing quantum mechanically path-entangled photon pairs has received considerable attention as an optical-measurement platform. Recently, we carried out a proof-of-concept experiment to show that ISUP can be used to measure the transmission spectrum of a Fabry-Perot resonator. Here, we demonstrate that ISUP with dual stimulated parametric down-conversion (StPDC) processes, which allows us to perform infrared rovibrational spectroscopy with visible photons. In our ISUP method, quantum coherence between two independent signal photons from each StPDC crystal is induced by the indistinguishability of conjugate idler fields and results in high visibility of the signal single-photon interferometry at the nondegenerate wavelength. If the seed-beam intensity is imbalanced due to the sample absorption, the corresponding envelope modulation of the interference fringe as a function of the seed-beam frequency reveals the absorption spectrum of the optical sample. As a proof-of-principle experiment, the full rovibrational transmission spectrum at 1550 nm of the hydrogen cyanide ($\text{H}^{13}\text{C}^{14}\text{N}$) molecules in a gas cell is measured from the single-photon interference fringe of the signal fields at 807 nm. We thus anticipate that the single-photon ISUP technique with dual StPDC crystals will find broad use for the development of high-resolution atomic and molecular spectroscopy with undetected photons.

DOI: 10.1103/PhysRevApplied.14.014045

I. INTRODUCTION

Various platforms for precision optical measurements utilizing quantum-entangled photon pairs have been developed over the past few decades for quantum spectroscopy [1–6], imaging [7–10], and metrology [11]. In particular, a pair of path-entangled photons from two sequential parametric down-conversion (PDC) processes that exhibits an induced single-photon quantum coherence has been used in various quantum erasing experiments without necessitating heralded detection [3,4,7,12–17], contrary to the conventional two-photon interference measurements by coincidence detection. Then, the introduction of an optical material (sample) to one arm of the idler path would alter the degree of indistinguishability of the idler fields generated from two PDC crystals in phase-sensitive single-photon interferometry (SPI) [3,7,12,13]. As a result,

the spectral information about the sample can be measured in SPI, consisting of the conjugate signal photons that never interact with the sample. This single-photon interference-based spectroscopy technique enables one to measure either the amplitude or phase changes of the idler field that interacts with materials through controlling the degree of which-way information without any temporal correlation detection of entangled signal-and-idler photon pairs. For infrared spectroscopy of CO_2 gas with visible light, for example, Kalashnikov *et al.* have investigated a proof-of-concept experiment based on the induced single-photon interference of frequency-entangled visible photons by using two cascaded *spontaneous* parametric down-conversion (SPDC) crystals [3]. The spectral resolution of the SPDC-based quantum spectroscopy, however, is limited in principle by the inherent broad bandwidths of the generated idler and signal fields. Thus, spectroscopic detection of the individual rovibrational transition of the gas-phase molecules with this method is technically tricky [3,12]. Thus, a spectroscopy method in SPI with high-resolution capability would find broad applications for atomic and molecular spectroscopy in various phases.

Recently, we demonstrated high-resolution interferometric spectroscopy with undetected photons (ISUP) with

*thyoon@korea.ac.kr

†mcho@korea.ac.kr

[‡]Present address: Quantum Technology Institute, Korea Research Institute of Standards and Science (KRISS), Daejeon 34113, Republic of Korea.

dual *stimulated parametric down-conversion* (StPDC) processes by employing a Fabry-Perot resonator as a test optical sample [4], where the line width of the seed laser limits the frequency resolution. In Ref. [4], the single-photon coherence of the signal photons is induced by erasing the which-way information of the conjugate idler photons via indistinguishability of the single-photon-added coherent states of two idler fields at the limits of the high seed-beam photon number ($n_i = |\alpha_i|^2 \gg 1$) and ultralow coupling of the pump beams [14,15]. This is in sharp contrast to the previous ISUP method with dual SPDC crystals, where the single-photon coherence is induced by erasing the which-way information of the idler fields at the single-photon level through aligning them collinearly [3,7,16,17]. Furthermore, our dual-StPDC-based ISUP method differs from the other optical-measurement techniques based on optical-frequency conversion [18–22], because our method uses quantum-correlated signal-idler photon pairs, where the entangled signal photons from different StPDC sources generate an interference fringe with unit visibility and its phase is modulated by the optical sample interacting with the seed beam. In the present work, we apply our proposed ISUP method with dual StPDC crystals for the high-resolution rovibrational spectroscopy of $\text{H}^{13}\text{C}^{14}\text{N}$ molecules in a gas phase. This experiment demonstrates that the proposed ISUP method indeed has a high-resolution capability, such that it is able to detect each individual rovibrational transition line of molecular gas, overcoming the spectral-resolution limit of the SPDC-based ISUP techniques. We anticipate that our proposed ISUP method can find further use for tomography and microscopy with undetected photons [23] at the single-photon level [24].

II. OPERATION PRINCIPLE OF ISUP

In this section, we describe the operation principle of the proposed ISUP with dual StPDC crystals. As illustrated in Fig. 1(a), our ISUP setup mainly consists of two parts, i.e., the detection section (dotted box) in which two StPDC crystals pumped by the same optical frequency comb (OFC) generate independent signal photons for SPI, as well as the spectroscopy section (solid box), in which an optical sample ($\text{H}^{13}\text{C}^{14}\text{N}$ gas) interacts with the frequency-tunable laser (seed). The extended optical layout of the experimental setup is described in Fig. 4 of Appendix A and the theory of SPI with dual StPDC crystals is described elsewhere [4,14] and summarized in Appendix A. Here, we briefly explain the main features of the SPI with dual StPDC crystals. Two nonlinear crystals (periodically poled lithium niobate, PPLN) are pumped by an OFC at the center wavelength of 530 nm with the optical bandwidth of 2.6 nm (10-ps pulse width), which is generated from the frequency doubling of a 1060-nm Yb fiber

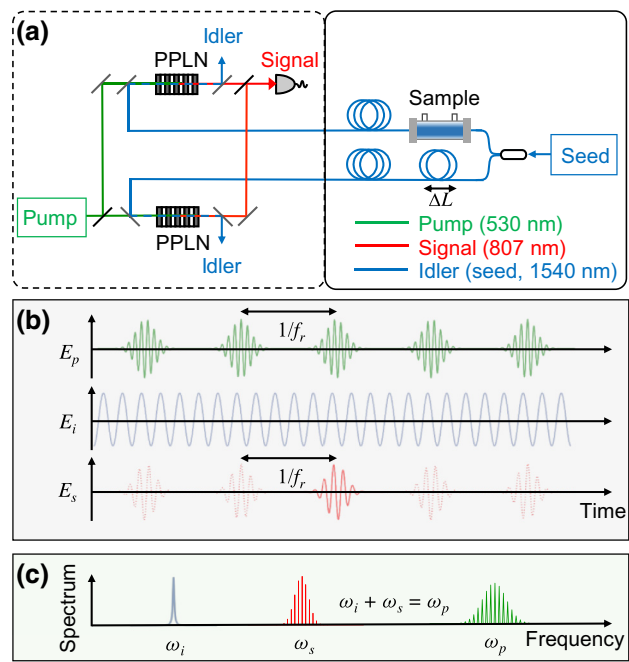


FIG. 1. (a) A schematic diagram of the interferometric spectroscopy with undetected photons (ISUP). Path-entangled and nondegenerate signal-idler photon pairs are generated from two identical PPLN crystals to form single-photon interferometry with signal photons (dotted box). Electric fields and optical spectra for the pump, idler (seed), and signal fields are depicted in (b) and (c). The pump beam, with amplitude E_p and center frequency ω_p , is an optical frequency comb (OFC) with a repetition frequency f_r , while the seed beam, with an amplitude E_i and frequency ω_i , is a continuous coherent laser. Then, the signal fields, of amplitude E_s and center frequency ω_s , have discrete frequencies satisfying the frequency relation $\omega_i + \omega_{s,m} = \omega_{p,m}$, where m is the mode number of the OFC. In an experiment with $|\Delta L| \neq 0$, only one of two seed beams interacts with the molecular sample (solid box), $\text{H}^{13}\text{C}^{14}\text{N}$, in the gas phase.

OFC with a repetition frequency, f_r , of 250 MHz and a carrier-envelope-offset frequency, f_{ceo} , of 20 MHz. These 2 rf degrees of freedom of the OFC are phase locked to the reference frequencies from a GPS-disciplined Rb atomic clock. The PDC efficiency at the pump and seed powers of 3 mW and $2.5 \mu\text{W}$, respectively, is very low. Thus the resulting signal field at the output of two StPDC crystals can be safely described as a single-photon state [4,14]. With these pump parameters, the detected single-photon count rate is measured to be 3×10^7 photons per second by using a single-photon-sensitive two-dimensional CCD array detector (EMCCD), which corresponds to 0.1 photons per pulse. As illustrated in Fig. 1(b) in the time domain and in Fig. 1(c) in the frequency domain, the train of generated signal pulses also consists of multiple discrete-frequency components, $f_{s,m} = m f_r + f_{\text{ceo}} - f_i$, with m denoting integers. In other words, each comb component of the pump OFC with mode number m and the

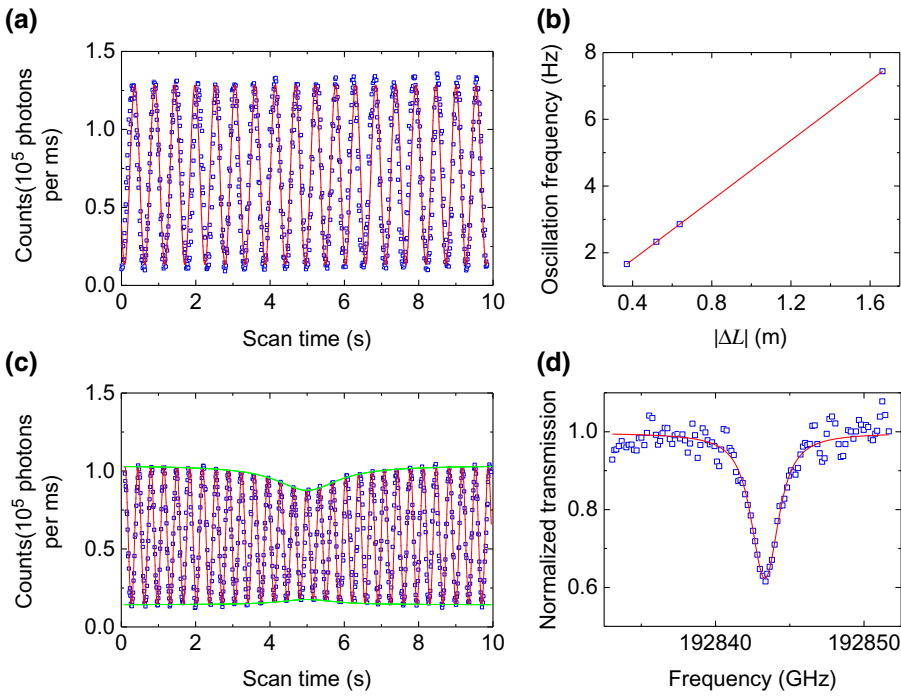


FIG. 2. (a) The photon count per 10 ms without an optical sample versus the frequency scan time ΔT with $|\Delta L| = 0.52$ m. (b) The oscillation frequency versus the path-length difference $|\Delta L|$ for $|\Delta L| = \{0.37$ m, 0.52 m, 0.64 m, 1.66 m $\}$. (c) The same as (a) but with $|\Delta L| = 1.66$ m in the presence of HCN molecules. Here, ω_i is tuned across the P16 rovibrational line ($\lambda = 1554.590\,79$ nm) and $\Delta\nu = 9.26$ MHz per 10 ms. The envelope (green line) is altered by the absorption of the H¹³C¹⁴N molecular resonance. (d) The transmittance spectrum (open square) of the P16 rovibrational transition retrieved from the interference fringe in (c); the solid line is its Voigt fit ($R^2 = 0.92$).

monochromatic seed field with a frequency of f_i generates single photons with a discrete spectrum satisfying the type-0 phase-matching condition and energy conservation of the StPDC process. Thus, the signal photons also form an OFC at the single-photon level in the frequency domain and a single-photon pulse train in the time domain [14,24].

Let us next consider the spectroscopy section depicted in the solid box of Fig. 1(a). The frequency-tunable seed beam with a narrow line width of approximately 10 kHz is split into two paths by a 50:50 fiber beam splitter and the upper seed beam interacts with the optical sample, i.e., H¹³C¹⁴N molecules in a fiber-coupled gas cell at 25 Torr and room temperature. Then, each seed beam is transferred to the detection section through 5-m-long polarization-maintaining optical fiber and used to stimulate idler photons at each PPLN crystal. Also, the seed-beam path-length difference $\Delta L = L_u - L_l$ can easily be made asymmetric by adjusting the upper-path fiber length L_u or lower-path fiber length L_l ; thus $|\Delta L|$ gives an additional degree of freedom that changes the phase-variation speed of the SPI [see Eq. (1) and Fig. 2], which can be adjusted to optimize the measurement efficiency of our ISUP method. In the experiment, the frequency of the injected seed beam can be scanned either discretely with a frequency step of 50 GHz or continuously within the range of ± 25 GHz. Thus, within the continuous-frequency-tuning range with a constant tuning rate η , the angular frequency of the seed beam can be written as $\omega_i(t) = 2\pi(f_i^0 + \eta t)$, where f_i^0 is the step-scanned laser frequency in an interval of 50 GHz. Then, when $\Delta L \neq 0$, a linear phase variation associated with the linear frequency tuning of the seed field is

given by

$$\Delta\phi_i(t) = 2\pi\eta t\Delta L n/c, \quad (1)$$

where c is the speed of light and n is the refractive index of the fiber. Thus, the total phase difference can be written as $\Delta\Phi_i(t) = \Delta\phi_{i0} + \Delta\phi_i(t)$, where $\Delta\phi_{i0}$ includes all other time-independent phase differences associated with the seed path difference. As will be shown below, this linear phase difference between the idler (seed) fields at each PPLN crystal results in the fast oscillation of the single-photon interference fringe generated by superposed signal fields from each PPLN crystal.

Then, the single-photon count R_s per integration time Δt of the interference fringe at the detector in Fig. 1 may be written as (see Appendix A) [14–16]

$$R_s(\Delta T) \propto I_1 [|\alpha(\omega_i)|^2 |T(\omega_i)|^2 + 1] + I_2 [|\alpha(\omega_i)|^2 + 1] \\ + 2 |\alpha(\omega_i)|^2 \sqrt{I_1 I_2} |T(\omega_i)| \cos [\Delta\phi_i(\Delta T) + \Delta\phi_0], \quad (2)$$

where $\Delta T = n\Delta t$ is the frequency scan time, n is an integer, I_j is the pump-beam intensity, and $|\alpha(\omega_i)|^2$ is the average number of photons of the seed beam. It is noted that the phase of the interference fringe in Eq. (2) can be altered by two terms: the phase difference $\Delta\phi_i(\Delta t)$ of Eq. (1) as well as $\Delta\phi_0 = \Delta\phi_{p0} + \Delta\phi_{s0} + \Delta\phi_{i0}$, a stationary phase factor associated with the constant pump, signal, and seed path-length differences. From Eq. (2), the visibility V of the single-photon interference fringe is

given by

$$V = \frac{2 |T(\omega_i)| |\alpha(\omega_i)|^2}{|\alpha(\omega_i)|^2 + |T(\omega_i)\alpha(\omega_i)|^2 + 2}, \quad (3)$$

when $I_1 = I_2$, i.e., the same pump-beam conditions for two StPDC crystals with the seed-beam photon numbers $|T(\omega_i)\alpha(\omega_i)|^2$ and $|\alpha(\omega_i)|^2$, respectively, at the upper and the lower PPLN crystals. This result shows that the measured fringe visibility depends not only on the transmission coefficient $|T(\omega_i)|$ of the optical sample but also on the average number of photons $|\alpha(\omega_i)|^2$ of the input seed beams [14]. The latter dependence can be understood by noting that the quantum state of the photon pair becomes a maximally path-entangled single-photon state as $|\alpha(\omega_i)|^2 \rightarrow 0$, which causes the visibility of the single-photon interference fringe to be zero. In the experiment, we choose $|\alpha(\omega_i)|^2 \approx 100$ per pump-pulse duration of 10 ps [4] to make $V(\Delta\omega_i) = 1$, in principle, at the idler frequency far off from the molecular resonance frequency ω_0 , i.e., $|\Delta\omega_i| = |\omega_i - \omega_0| \gg 0$.

III. MOLECULAR ROVIBRATIONAL SPECTROSCOPY WITH UNDETECTED PHOTONS

Now, we present the experimental demonstration of our ISUP method with dual StPDC crystals for rovibrational spectroscopy using the setup in Fig. 1(a) (see also Fig. 4). If we take into account the experimental conditions for ISUP, i.e., equal pump-beam intensities ($I_1 = I_2$) and single-photon interference with high visibility ($|\alpha(\omega_i)|^2 \gg 1$), we have the single-photon counting rate from Eqs. (2) and (3) as

$$R_s(\Delta\nu) \approx \frac{R_0}{4} [1 + |T(\Delta\nu)|^2] \{1 + V \cos [\Delta\phi_i(\Delta\nu) + \Delta\phi_0]\}, \quad (4)$$

where $\Delta\nu = \eta\Delta t$ is the frequency step per integration time Δt and $R_0 \approx 1.25 \times 10^8$ is the measured single-photon count per second [see, e.g., Fig. 2(a)]. From Eq. (4), we see that $R_s(\Delta\nu) \approx R_0/2 \{1 + V \cos [\Delta\phi_i(\Delta\nu) + \Delta\phi_0]\}$, when there is no optical sample or $|\Delta\omega_i| \gg 0$, i.e., $|T(\Delta\nu)| = 1$. To verify that our SPI has a high phase sensitivity for fixed η and ΔL without an optical sample, we measure R_s with respect to the seed-frequency scanning time ΔT , as shown in Fig. 2(a). We find here that the oscillation frequency of the signal $R_s(\Delta T)$ is proportional to ΔL as expected from Eqs. (1) and (4) and confirmed experimentally in Fig. 2(b). From Fig. 2(b), it becomes clear that the phase sensitivity of our frequency-comb SPI can be enhanced with a longer path-length difference $|\Delta L|$ for a given scan rate.

After the optical sample is inserted, we again measure R_s as a function of ΔT , when the seed-beam frequency

is tuned across the $P16$ rovibrational transition of the $H^{13}C^{14}N$ molecules ($\lambda = 1554.590\,79$ nm) as shown in Fig. 2(c), with $|\Delta L| = 1.66$ m. In Fig. 2(c), the frequency scan rate η is set to be 0.926 GHz/s. Thus, the frequency-tuning step $\Delta\nu$ per integration time of 10 ms is 9.26 MHz. Notably, the scanning time- or seed-frequency-dependent envelope of the fringe (green line) is altered by the presence of the optical sample. This is because the intensity attenuation of the seed beam by the absorptive HCN molecules in the gas cell modulates the distinguishability of the quantum-entangled signal fields in the upper and lower paths of our frequency-comb SPI. In order to extract the spectral information $|T(\Delta\nu)|$, we first determine the visibility V_m at $|\Delta\omega_i| \gg 0$ from Eq. (4) and Fig. 2(c), i.e., $V_m = (R_{s,\max} - R_{s,\min})/R_0 \approx 0.88$, where $R_{s,\max}(R_{s,\min})$ is the maximum (minimum) value of $R_s(\Delta\omega)$ at the far-off detuning frequency. The measured visibility V_m is slightly off from unity due to the insertion of the sample cell. Then, we can measure $|T(\Delta\nu)|$ from the measured values of $R_s(\Delta T)$ near resonance, i.e., $\Delta\omega_i \approx 0$, from the relation $|T(\Delta\nu)| = \sqrt{2/R_0 (R_{s,\max} + R_{s,\min})} - 1$. To get the fine transmission spectrum, however, it is also possible to find $|T(\Delta\nu)|$ by fitting the experimental data in Fig. 2(c) with Eq. (4) near the molecular resonance frequency with $V = V_m$. The transmittance spectrum of the $P16$ line retrieved in this way is shown in Fig. 2(d) (open square) and the solid line is its Voigt fit.

The experimental results in Fig. 2 demonstrate the capability of our ISUP method with dual StPDC crystals for high-resolution rovibrational spectroscopy with undetected photons. Specifically, it measures the complex near-IR susceptibility of molecular systems with high phase sensitivity having a frequency-converted single-photon counting feature, e.g., the seed-beam absorption at approximately 1550 nm is directly transferred to the interference-fringe modulation of the signal SPI at approximately 810 nm. This wavelength-converted counting capability of our dual-StPDC-based ISUP method enables us to measure the entire vibrational spectra of the $H^{13}C^{14}N$ molecular gas by merely tuning the seed-beam frequency across the whole wavelength span of the HCN rovibrational transitions.

In Fig. 3, we summarize the ISUP-measured complete transmission lines belonging to both the R and P branches of the $H^{13}C^{14}N$ rovibrational transitions in the wavelength range from 1528 nm to 1566 nm. The center wavelength of the StPDC-generated signal field varies from 801 to 812 nm when we tune the seed-beam wavelength (see Fig. 5). This result is understandable from the fact that the wavelengths (frequencies) of the tunable seed and the generated signal beams from the phase-matched PPLN crystal are anticorrelated when the spectrum of the pump beam is fixed (see Appendix C). The entire spectrum in Fig. 3(a) results from the reconstruction of

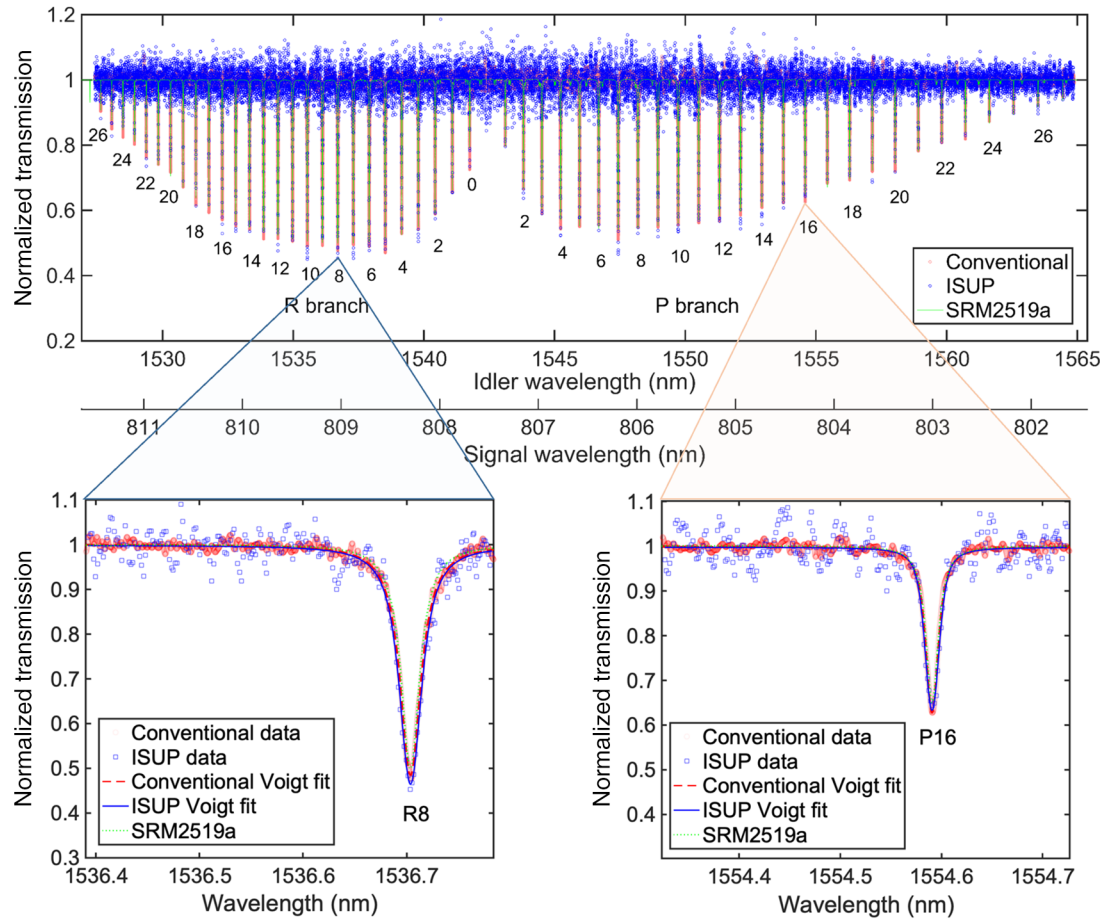


FIG. 3. (a) The complete rovibrational transmission spectra of $\text{H}^{13}\text{C}^{14}\text{N}$ molecules measured with a 16.5-cm gas cell at 25 Torr and room temperature. The blue and red dots are, respectively, measured by the ISUP method and conventional spectroscopy. The peak frequency of each rovibrational line is calibrated from NIST SRM2519a for $\text{H}^{13}\text{C}^{14}\text{N}$ molecular gas in a 15-cm gas cell at a pressure of 25 Torr (solid green line). The spectrum shown in (a) is constructed from 50 separately measured spectra. (b) The expanded spectrum of the $R8$ ($\lambda = 1536.704 \text{ nm}$) and $P16$ ($\lambda = 1554.59079 \text{ nm}$) lines with line widths of 2.8 GHz and 2.2 GHz, respectively. The solid blue and dashed red lines are Voigt fits ($R^2 = 0.97$ and 0.96 for $R8$ and $P16$, respectively) and the green dotted lines are from SRM2519a.

more than 50 rovibrational lines measured separately by changing the center frequency of the seed beam with an interval of 50 GHz. The blue dots in Fig. 3 are the measured ISUP spectrum and the red dots correspond to the spectrum independently measured for comparison using a conventional spectrometer, meaning here that the probe and detection wavelengths are the same, with the same seed laser and a photodetector with high sensitivity at $1.5 \mu\text{m}$. The center wavelength of each line is calibrated to that from the NIST SRM2519a(15-cm $\text{H}^{13}\text{C}^{14}\text{N}$ cell at 25 Torr and room temperature) [25]. Two representative rovibrational lines, $R8$ and $P16$, are shown in Fig. 3(b) and they have signal-to-noise ratios of 15 and 10, respectively. The measured line widths of 2.8 GHz for $R8$ and 2.2 GHz for $P16$ lines originate from the convolution of homogeneous pressure broadening and inhomogeneous Doppler broadening (approximately 450 MHz). To further

compare our experimental results with the NIST SRM data at different pressures, we measure the same rovibrational line, $P16$, at two different pressures, i.e., 25 Torr and 100 Torr, with the same cell length of 16.5 cm (Appendix E). They are in quantitative agreement with the SRM data as well. It should be pointed out that not only are the line widths of the transmission lines at the same pressure and temperature across the whole R and P branches of the rovibrational transitions of the $\text{H}^{13}\text{C}^{14}\text{N}$ molecules in Fig. 3 but the absorption strength of each transition line agrees well with that of the SRM data. Thus, from the experimental results in Fig. 3, it becomes clear that the dual-StPDC-based ISUP technique demonstrated in this work presents rovibrational-resolved molecular spectroscopy with undetected photons in the gas phase and has the potential to be used for high-resolution atomic and molecular spectroscopy covering various spectral ranges

by the wavelength-converted detection technique at the single-photon level.

IV. FEATURES OF ISUP

Finally, we want to emphasize the features of our ISUP method for the rovibrational spectroscopy compared to other approaches. First, our ISUP method demonstrated in the present work has a high-frequency resolution limited only by the line width of the seed laser. It can be understood by noting that we use a narrow-band seed laser in an idler mode near $1.55\ \mu\text{m}$ to stimulate the two PDC processes to generate two independent single-photon sources in the signal mode near $807\ \text{nm}$ for interferometric detection of undetected photons by the induced coherence (see Fig. 1), which is substantially different from other methods. For example, the Krivitsky group [3] have employed two spontaneous PDC processes for IR spectroscopy with undetected photons. This difference in the way of generating two pairs of signal-idler photons, i.e., stimulated PDC with two (pump and seed) lasers versus spontaneous PDC with just one (pump) laser, makes some huge differences: (i) an improvement of the PDC efficiency via induced emission in the low pumping limit, by a few orders of magnitude, (ii) an enhanced frequency resolution with a narrow-band seed laser, (iii) the possibility of remote spectroscopy due to the separability of the measurement and probing parts of our setup, and (iv) controllability of the signal photon interferometry from the classical to the quantum regime via adjusting the power of seed beam in an idler mode. Thus the generated idler field in our case is a single-photon-added coherent state (SPACS), whereas that in the work of the Krivitsky group is a one-photon Fock state. Thus, the experimental details of our approach are significantly different from those reported by the authors of Ref. [3]. In addition, our ISUP method has an enhanced SNR due to the common noise cancellation in the single-photon interferometry involving two identical StPDC crystals. The induced coherence between a pair of signal photons from two independent StPDC crystals originates from the statistical indistinguishability of the SPACS of the conjugated idler photons at the limit of the high coherent amplitude of the seed beam. For high-resolution rovibrational spectroscopy, we continuously scan the wavelength of the seed beam across each rovibrational molecular transition and then the modulated visibility of the single-photon interference fringe due to the molecular absorption reveals the molecular-absorption spectra. Furthermore, we use an optical-frequency comb as the pump source for the two StPDC crystals and a narrow-line-width seed beam at the idler wavelength, resulting in the optical-frequency comb at the signal wavelength, consisting of a few photons per mode. This frequency-comb signal field [14] could be of use for the development of quantum OFC spectroscopy in the future.

V. CONCLUSION

In summary, we demonstrate rovibrational spectroscopy with undetected photons for $\text{H}^{13}\text{C}^{14}\text{N}$ molecules in the gas phase. In the proposed ISUP technique, we use an optical frequency comb as the pump source and a coherent cw laser as the seed and spectroscopy beam at the idler wavelength for two StPDC crystals to generate quantum-correlated signal photons for the SPI operating at the nondegenerate visible wavelength. The differential absorption of one of the seed beams by the $\text{H}^{13}\text{C}^{14}\text{N}$ molecules, depending on the seed-beam frequency, results in the high-resolution measurement of the individual rovibrational spectrum. We anticipate that the efficient single-photon detection by the greatly enhanced single-photon emission rate in the dual-StPDC-based ISUP method beyond the spectral range specific to the optical material will be of particular use for the development of frequency-resolved spectroscopy and microscopy with undetected photons.

ACKNOWLEDGMENTS

This work was supported by IBS-R023-D1. T.H.Y. was supported in part by 2019R1A2C2009974.

APPENDIX A: THEORY OF THE ISUP METHOD WITH DUAL STPDC CRYSTALS

In a SPDC process, a two-mode squeezed vacuum state, i.e., a well-known photon-number entangled state, is generated [26,27]. Because the conversion efficiency of the SPDC process is extremely low in the weak-coupling regime, it is safe to ignore all the multiphoton-generation events except for the generation of a single pair of signal-and-idler photons. In the present work, we consider a stimulated PDC (StPDC) process in the weak coupling limit, where the pump is down-converted by the stimulation process, with a coherent seed beam in the idler mode. Then, the signal field is initially in a vacuum state and the idler field is initially in a coherent state with frequency ω_i and complex amplitude $\alpha(\omega_i)$. Thus, the initial composite quantum state for the signal and idler fields can be written as $|\psi(0)\rangle = |0\rangle_s |\alpha(\omega_i)\rangle_i$ and a two-mode squeezed coherent state is generated by the StPDC process. In this low-coupling limit, the quantum state of the bipartite system can be approximately described as a product of the single-photon state in signal mode and single-photon-added coherent state (SPACS) [28] in the idler mode, i.e., $|1\rangle_s \hat{a}_i^\dagger |\alpha(\omega_i)\rangle_i$, where \hat{a}_i^\dagger is the creation operator of idler photons.

To develop a theory for the dual-StPDC-based SPI in Figs. 1(a) and 4, we first consider the time-dependent quantum state under the influence of the StPDC interaction Hamiltonian in the weak-coupling regime,

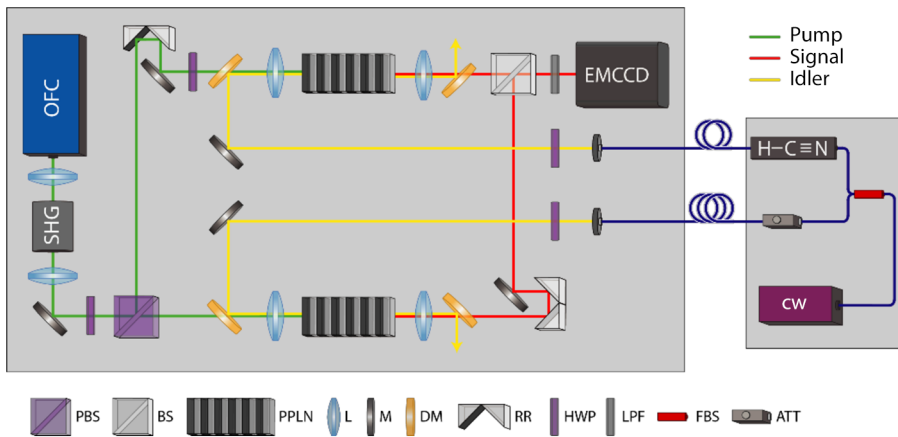


FIG. 4. The experimental setup of the ISUP method with dual StPDC crystals for molecular spectroscopy with undetected photons: OFC, optical frequency comb; SHG, second-harmonic generation; EMCCD, electron-multiplying charge-coupled device; cw, continuous wave, H-C≡N; H¹³C¹⁴N; PBS, polarization beam splitter; BS, beam splitter; PPLN, periodically poled lithium niobate; L, lens; M, mirror; DM, dichroic mirror; RR, retroreflector; HWP, half-wave plate; LPF, long-pass filter; FBS, fiber beam splitter; ATT, attenuator.

$\hat{H}_I = i\hbar g E_p(\omega_p, t) \hat{a}_s^\dagger(\omega_s) \hat{a}_i^\dagger(\omega_i) + h.c.$, which can be approximately written as

$$|\psi(t)\rangle \simeq \left[1 - \frac{i}{\hbar} \int \hat{H}_I(t) dt \right] |0\rangle |\alpha(\omega_i)\rangle_i, \quad (\text{A1})$$

where g is the coupling coefficient, which is proportional to the second-order susceptibility $\chi^{(2)}$ of the PDC crystal, E_p is the complex amplitude of the pump beam, $\hat{a}_{s,i}^\dagger$ ($\hat{a}_{s,i}$) is the creation (annihilation) operator for the signal (s) and idler (i) photons, and $\mathcal{F}(\omega_s, \omega_i)$ is the joint spectral function determined by the phase-matching condition of the nonlinear crystal. Because the PDC is a parametric process, the frequency of the generated signal photon is given as $\omega_s = \omega_p - \omega_i$. Here, the signal beam has multiple frequency-comb components, i.e., $\omega_{p,m} = \omega_c + 2\pi m f_r$, with m denoting integers, where $\omega_c = 2\pi(m_{fr} + f_{ceo})$ is the center frequency of the pump beam, m_c is its mode number, f_r is the repetition frequency of the pulse train, and f_{ceo} is the carrier-envelope-offset frequency [14].

In our dual-StPDC-based SPI, two identical nonlinear crystals are pumped by the same OFCs and their idler photons are stimulated by the same seed beams but only one of two idler beams is allowed to interact with the optical sample. In the low-coupling-efficiency regime, i.e., $|g_j t E_{p,j}|^2 |\alpha_j(\omega_i)|^2 \ll 1$, where $j = 1(2)$ refers to the upper (lower) path, the resulting composite quantum state in the dual-StPDC-based SPI, $|\psi(t)\rangle = |\psi(t)\rangle_1 \otimes |\psi(t)\rangle_2$, is approximately given as

$$|\psi(t)\rangle \approx |1, 0\rangle_{s_1, s_2} \hat{a}_{i,1}^\dagger |T(\omega_i)\alpha_1(\omega_i), \alpha_2(\omega_i)\rangle_{i_1, i_2} \\ + |0, 1\rangle_{s_1, s_2} \hat{a}_{i,2}^\dagger |T(\omega_i)\alpha_1(\omega_i), \alpha_2(\omega_i)\rangle_{i_1, i_2} \quad (\text{A2})$$

after omitting the vacuum state and ignoring the probability of simultaneous generation of two signal-idler photon pairs by each StPDC crystal [4,14]. Then, the single-photon interference fringe (or single-photon count rate) of the superposed signal photons after the beam combiner can be calculated as $R_s = \langle \psi(t) | E_s^- E_s^\dagger | \psi(t) \rangle$, where

$E_s^\dagger = \sum_{\omega_s} [e^{i\varphi_{s1}} \hat{a}_{s1}(\omega_s) + e^{i\varphi_{s2}} \hat{a}_{s2}(\omega_s)]$, $E_s^- = (E_s^\dagger)^\dagger$ and φ_{sj} is the phase acquired by the j th signal field. Since $T(\omega_i)\alpha(\omega_i) \neq \alpha(\omega_i)$ due to the sample absorption, R_s could be written as [14–16]

$$R_s \propto I_1 [|\alpha(\omega_i)|^2 |T(\omega_i)|^2 + 1] + I_2 [|\alpha(\omega_i)|^2 + 1] \\ + 2 |\alpha(\omega_i)|^2 \sqrt{I_1 I_2} |T(\omega_i)| \cos \left[\sum_{k=p, s, i} \Delta\varphi_k \right], \quad (\text{A3})$$

where the pump-beam intensity is denoted as $I_j = |E_{p,j}|^2$ and the phase differences of the pump (p), seed (or idler, i), and signal (s) fields are defined as $\Delta\varphi_k = \varphi_{k1} - \varphi_{k2}$. From Eq. (A3), the expression for the fringe visibility can be obtained as Eq. (3) in the main text when the two pump intensities are the same, i.e., $I_1 = I_2$. Equation (A3) indicates that both the measured photon count rate at the detector and the fringe visibility depend on (i) the transmission spectrum $T(\omega_i)$ of the optical sample at the idler frequency ω_i , (ii) the frequency-dependent average photon number of the seed beam, i.e., $|\alpha(\omega_i)|^2$, and (iii) the path-length differences of the pump, seed, and signal beams in the interferometry. The most important aspect of our dual-StPDC-based SPI is that the fringe visibility in Eq. (3) of the signal field at 807 nm can be modulated by the intensity imbalance, i.e., $T(\omega_i)\alpha(\omega_i) \neq \alpha(\omega_i)$, between two seed beams at 1.54 μm in the idler mode. As experimentally demonstrated in the present ISUP experiments, $|T(\omega_i)|$ can thus be obtained by analyzing the experimentally measured single-photon interference fringe of the signal photons with Eq. (4) in the main text.

APPENDIX B: DETAILS OF THE ISUP EXPERIMENTAL SETUP

An optical frequency comb (OFC) pump at 530 nm with a spectral bandwidth of 2.6 nm and temporal pulse width of 10 ps is prepared from the second-harmonic generation (SHG) of a fundamental OFC laser (Menlo Systems) at

1060 nm with a spectral bandwidth of 40 nm. An lithium triborate crystal (Newlight Photonics, $3 \times 5 \times 5 \text{ mm}^3$, type I phase-matching temperature of 143°C) is used for the SHG. The repetition frequency and carrier-envelope-offset frequency of the fundamental OFC are actively stabilized at 250 MHz and 20 MHz, respectively, by using a GPS-disciplined Rb atomic clock. The 6-mW pump beam is divided into two beams and their relative intensities are controlled by using a half-wave plate (HWP) and a polarizing beam splitter (PBS). Each pump beam is focused onto a periodically poled lithium-niobate (PPLN) crystal (HCP, type-0, $15 \times 7.9 \times 0.5 \text{ mm}^3$, grating width of $7.3 \mu\text{m}$) by using an achromatic lens with a focal length of 100 mm. Both the pump and seed beams are vertically polarized to satisfy the type-0 phase-matching condition.

A portion of coherent cw light along the upper path is fiber coupled to the optical sample of the ($\text{H}^{13}\text{C}^{14}\text{N}$) molecules in a fiber-coupled gas cell (Wavelength Reference, 25 Torr, 16.5 cm), and the total length difference between two seed-beam paths is set to be nonzero, i.e., $\Delta L \neq 0$. Two seed beams are then guided to two PPLN crystals by using 5-m-long PM fibers and used to stimulate idler photons at two PDC crystals pumped by two OFC lasers. The transmitted seed beam from the PPLN crystal is separated from the signal beam path by using a dichroic mirror (DM). Then, signal photons from two PPLN crystals are combined by the beam combiner for the generation of single-photon interference fringes. To obtain high-contrast interference fringes, we optimize the overlaps of two signal beams in the spectral, spatial, and temporal domains [4,14].

The interference fringe produced by the two signal fields is then detected by a single-photon-sensitive two-dimensional EMCCD camera (Andor Technology) attached to the output port of the spectrometer (Shamrock SR-303i-B, Andor Technology, grating 600 lines/mm at 500-nm blaze). The spectrometer is used not only to measure the center wavelength of the generated signal photons with a wavelength resolution of 0.02 nm but also for wavelength-selected single-photon counting during an integration time of 10 ms by the EMCCD camera attached to the exit of the spectrometer. Note that the integration time of 10 ms is much longer than the pulse-to-pulse time interval of 4 ns and slightly longer than the coherence time of the generated single fields [14].

APPENDIX C: JOINT-SPECTRAL-INTENSITY PLOT OF PPLN CRYSTAL

In the experiment, a pair of path-entangled photons are generated from two identical PPLN crystals via the type-0 phase-matching nondegenerate PDC process. The joint spectral intensity for the SPDC process is given

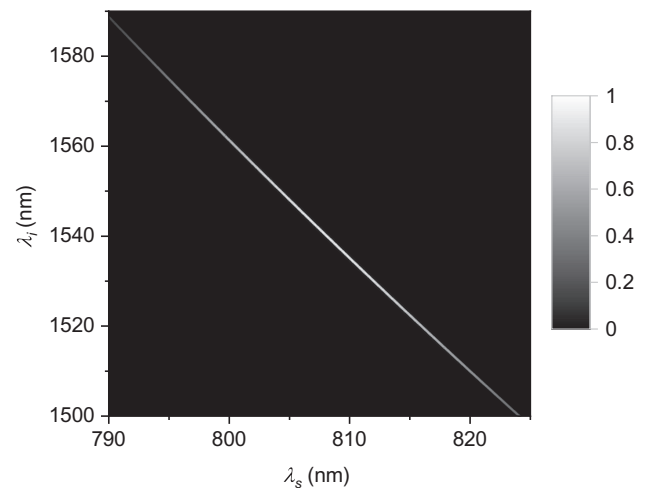


FIG. 5. The joint spectral intensity of the signal-idler photon pair for the type-0 phase-matching SPDC process in PPLN crystal. Gaussian pump-beam parameters at 530 nm with a spectral width of 2.6 nm and the Sellmeier equation of the PPLN crystal with a poling period of $7.3 \mu\text{m}$ at 121°C are used for the calculation.

as [14,29,30]

$$|\mathcal{F}(\omega_s, \omega_i)E_p(\omega_s + \omega_i)|^2 \propto \left| \text{sinc}\left(\frac{\Delta kl}{2}\right)\mathcal{E}_p \exp\left[-\left(\frac{c/\lambda_s + c/\lambda_i}{\sigma_p}\right)^2\right] \right|^2, \quad (\text{C1})$$

where $\Delta k = k_p - k_s - k_i$ is the wave-number mismatch, l is the length of the PPLN crystal, E_p is the pump electric field with Gaussian amplitude \mathcal{E}_p , and σ_p is the pump spectral width. The calculated joint spectral intensity as a function of the signal and idler wavelengths is shown in Fig. 5. For this calculation, the Sellmeier equation of the PPLN crystal for noncritical phase matching [31] and Gaussian pump-beam parameters are used, i.e., the center wavelength of 530 nm and the spectral width of 2.6 nm. Indeed, the joint-spectral-intensity plot shows a wide phase-matched spectral width of the nondegenerate signal and idler photons at the phase-matching temperature of 121°C , supporting the measured wavelength anticorrelation of the idler and signal wavelengths of the rovibrational transition lines in Fig. 3(a) for a fixed pump wavelength at 530 nm with 2.6 nm spectral width.

APPENDIX D: ISUP WITH FREQUENCY STEP-SCAN METHOD

As shown in Fig. 2 in the main text, the proposed ISUP method works when the seed-beam frequency is scanned linearly with a constant rate η . Equation (4), however, also suggests that the ISUP method should work equally when $\eta = 0$, i.e., the frequency of the seed beam is scanned

stepwise and stabilized during the integration time for photon count $R_s(\Delta t)$ (the frequency step-scan method, FSM), because the StPDC process is phase sensitive. In the FSM, either $\Delta\phi_p$ or $\Delta\phi_s$ can be linearly scanned instead. To confirm that the FSM is useful and quantitatively reliable for molecular ISUP, we independently measure $|T(\omega_i)|$ in Fig. 6(a) for the R8 rovibrational line of the HCN molecules in the gas phase. Here, the stabilized-frequency of the seed beam is tuned with an interval of 100 MHz in a stepwise manner. Also shown in Fig. 6(a) are the same spectra measured by the conventional interferometer (red square) and from the SRM2519a (green square) for comparison. In Fig. 6(b), the path-length difference of pump beam Δx_p , i.e., $\Delta\phi_p$ in Eq. (A3) is linearly scanned by using a piezoelectric transducer [4] and three representative interference fringes are shown at three different seed frequencies, i.e., (i) 195.0840 THz, (ii) 195.0866 THz, and (iii) 195.0880 THz, respectively, across the R8 rovibrational transition frequency. As expected, the fringe visibility becomes smaller as the transmittance of the optical sample decreases due to the molecular absorption. The transmittance extracted from the interference fringe in Fig. 6(b) from Eq. (4) is in quantitative agreement with those values obtained by using the continuous-scanning method discussed in the main text.

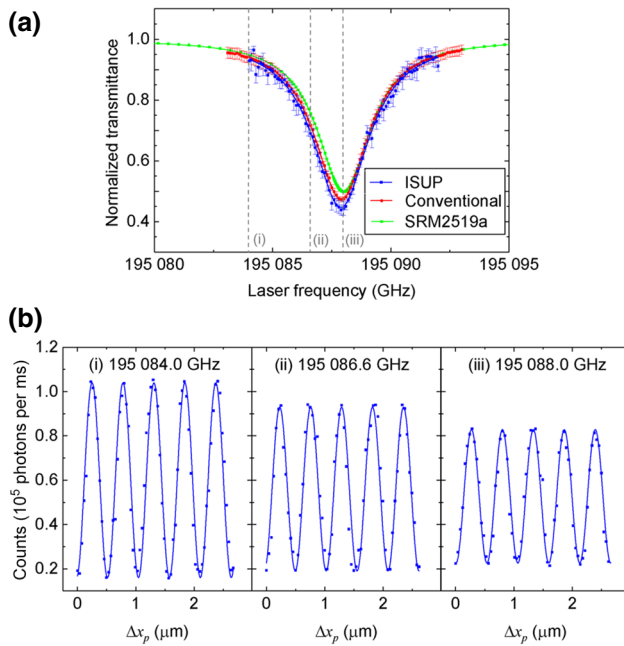


FIG. 6. (a) The normalized spectrum of the R8 rovibrational transition of HCN molecules (blue square) measured by the frequency step-scan method. (b) Three representative interference fringes are shown at three different seed frequencies: (i) 195.0840 THz, (ii) 195.0866 THz, and (iii) 195.0880 THz, respectively.

APPENDIX E: PRESSURE DEPENDENCE OF THE SPECTRAL WIDTH

Figure 7 compares the normalized transmission spectra of the (a) P16 and (b) R8 rovibrational transitions of the $\text{H}^{13}\text{C}^{14}\text{N}$ molecules measured at two different pressures at 25 Torr (3.3 kPa) and 100 Torr (13.3 kPa), respectively. The blue squares and gray up-triangles correspond to the spectra obtained by the ISUP method at 25 Torr and at 100 Torr, respectively. The solid lines are Voigt fits for each spectrum, with R^2 values of (a) 0.96 (25 Torr) and 0.94 (100 Torr) for P16 and (b) 0.94 (25 Torr) and 0.97 (100 Torr) for R8 (b), respectively. The green

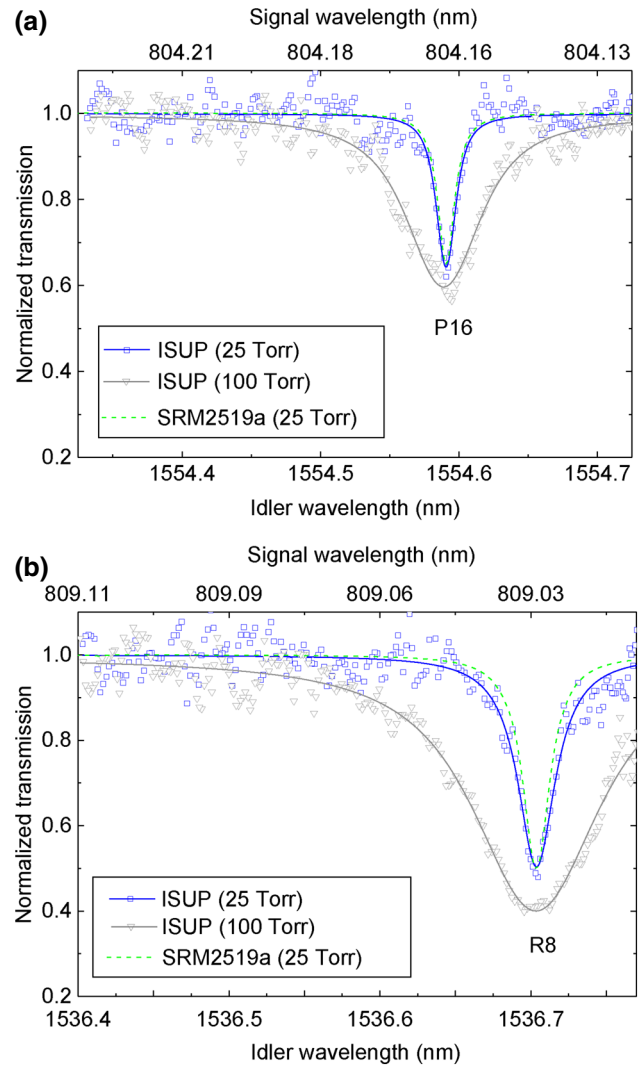


FIG. 7. A comparison of the normalized transmission spectra of the (a) P16 and (b) R8 rovibrational transitions of the $\text{H}^{13}\text{C}^{14}\text{N}$ molecules measured at two different pressures of 25 Torr (3.3 kPa) and 100 Torr (13.3 kPa), respectively. The coefficient-of-determination values for the Voigt fits are (a) $R^2 = 0.96$ (25 Torr) and 0.94 (100 Torr) for P16 and (b) 0.94 (25 Torr) and 0.97 (100 Torr) for R8, respectively.

dashed-dotted lines in Figs. 7(a) and 7(b) are the spectra of the SRM2519a at 25 Torr. One can see that the spectra at 100 Torr have significantly broader line widths, i.e., (a) 17 pm at 25 Torr and 30 pm at 100 Torr for *P*16 and (b) 65 pm at 25 Torr and 100 pm at 100 Torr for *R*8, respectively, due to the collision-induced homogeneous line broadening. The absorption depth also increases as the gas pressure is increased and its ratios depend on the transition-line strength. In Fig. 7, we take into account the pressure-shift coefficients of -0.139 pm/kPa and -0.021 pm/kPa for (a) *P*16 and (b) *R*8, respectively, to match the center frequencies of the two spectra. Figure 7 suggests that the present ISUP technique for rovibrational spectroscopy is sensitive enough to study collision-induced line broadening of the $1.5\ \mu\text{m}$ absorption line through examining the 800-nm signal-photon interference pattern, which is an experimental demonstration of quantum spectroscopy with undetected photons utilizing dual-StPDC single-photon interferometry.

- [1] G. Scarcelli, A. Valencia, S. Gompers, and Y. Shih, Remote spectral measurement using entangled photons, *Appl. Phys. Lett.* **83**, 5560 (2003).
- [2] A. Yabushita and T. Kobayashi, Spectroscopy by frequency-entangled photon pairs, *Phys. Rev. A* **69**, 013806 (2004).
- [3] D. A. Kalashnikov, A. V. Paterova, S. P. Kulik, and L. A. Krivitsky, Infrared spectroscopy with visible light, *Nat. Photonics* **10**, 98 (2016).
- [4] S. K. Lee, T. H. Yoon, and M. Cho, Interferometric quantum spectroscopy with undetected photons via distinguishability modulation, *Opt. Express* **27**, 14853 (2019).
- [5] C. Altuzarra, S. Vezzoli, J. Valente, W. Gao, C. Soci, D. Faccio, and C. Couteau, Coherent perfect absorption in metamaterials with entangled photons, *ACS Photonics* **4**, 2124 (2017).
- [6] R. D. J. León-Montiel, J. Svozilík, J. P. Torres, and A. B. U'Ren, Temperature-Controlled Entangled-Photon Absorption Spectroscopy, *Phys. Rev. Lett.* **123**, 023601 (2019).
- [7] G. B. Lemos, V. Borish, G. D. Cole, S. Ramelow, R. Lapkiewicz, and A. Zeilinger, Quantum imaging with undetected photons, *Nature* **512**, 409 (2014).
- [8] R. Tenne, U. Rossman, B. Rephael, Y. Israel, A. Krupinski-Ptaszek, R. Lapkiewicz, Y. Silberberg, and D. Oron, Super-resolution enhancement by quantum image scanning microscopy, *Nat. Photonics* **13**, 116 (2019).
- [9] T. B. Pittman, Y. H. Shih, D. V. Strekalov, and A. V. Sergienko, Optical imaging by means of two-photon quantum entanglement, *Phys. Rev. A* **52**, R3429 (1995).
- [10] S. P. Walborn, C. H. Monkenb, S. Páduab, and P. H. Souto Ribeiro, Spatial correlations in parametric down-conversion, *Phys. Rep.* **495**, 87 (2010).
- [11] F. Hudelist, J. Kong, C. Liu, J. Jing, Z. Y. Ou, and W. Zhang, Quantum metrology with parametric amplifier-based photon correlation interferometers, *Nat. Commun.* **5**, 3049 (2014).
- [12] A. Paterova, H. Yang, C. An, D. Kalashnikov, and L. Krivitsky, Measurement of infrared optical constants with visible photons, *New J. Phys.* **20**, 043015 (2018).
- [13] A. V. Paterova, S. M. Maniam, H. Yang, G. Grenci, and L. A. Krivitsky, Hyperspectral infrared microscopy with visible light, arXiv:2002.05956 (2020)..
- [14] S. K. Lee, N. S. Han, T. H. Yoon, and M. Cho, Frequency comb single-photon interferometry, *Commun. Phys.* **1**, 51 (2018).
- [15] Z. Y. Ou, L. J. Wang, X. Y. Zou, and L. Mandel, Coherence in two-photon down-conversion induced by a laser, *Phys. Rev. A* **41**, 1597 (1990).
- [16] L. J. Wang, X. Y. Zou, and L. Mandel, Induced coherence without induced emission, *Phys. Rev. A* **44**, 4614 (1991).
- [17] S. K. Lee, T. H. Yoon, and M. Cho, Quantum optical measurements with undetected photons through vacuum field indistinguishability, *Sci. Rep.* **7**, 6558 (2017).
- [18] Y.-H. Cheng, T. Thomay, G. S. Solomon, A. L. Migdall, and S. V. Polyakov, Statistically background-free, phase-preserving parametric up-conversion with faint light, *Opt. Express* **23**, 18671 (2015).
- [19] T. W. Neely, L. Nugent-Glandorf, F. Adler, and S. A. Diddams, Broadband mid-infrared frequency upconversion and spectroscopy with an aperiodically poled LiNbO₃ waveguide, *Opt. Lett.* **37**, 4332 (2012).
- [20] Q. Hu, J. S. Dam, C. Pedersen, and P. Tidemand-Lichtenberg, High-resolution mid-IR spectrometer based on frequency upconversion, *Opt. Lett.* **37**, 5232 (2012).
- [21] T. A. Johnson and S. A. Diddams, Mid-infrared upconversion spectroscopy based on a Yb:fiber femtosecond laser, *Appl. Phys. B* **107**, 31 (2012).
- [22] J. S. Dam, P. Tidemand-Lichtenberg, and C. Pedersen, Room-temperature mid-infrared single-photon spectral imaging, *Nat. Photonics* **6**, 788 (2012).
- [23] I. Kviatkovsky, H. M. Chrzanowski, E. G. Avery, H. Bartolomaeus, and S. Ramelow, Microscopy with undetected photons in the mid-infrared, arXiv:2002.05960 (2020).
- [24] N. Picqué and T. W. Hänsch, Single-photon interferometry and spectroscopy with two laser frequency combs, arXiv:1906.03706 (2019).
- [25] S. L. Gilbert, W. C. Swann, and C.-M. Wang, Hydrogen cyanide H¹³C¹⁴N absorption reference for 1530 nm to 1565 nm wavelength calibration—SRM 2519a, NIST Spec. Publ. **260**, 137 (2005).
- [26] C. T. Lee, Nonclassical photon statistics of two-mode squeezed states, *Phys. Rev. A* **42**, 1608 (1990).
- [27] S. L. Braunstein and P. V. Loock, Quantum information with continuous variables, *Rev. Mod. Phys.* **77**, 513 (2005).
- [28] A. Zavatta, S. Viciani, and M. Bellini, Quantum-to-classical transition with single-photon-added coherent states of light, *Science* **306**, 660 (2004).
- [29] S.-Y. Baek and Y.-H. Kim, Spectral properties of entangled photons generated via type-I frequency-nondegenerate spontaneous parametric down-conversion, *Phys. Rev. A* **80**, 033814 (2009).
- [30] C. K. Hong and L. Mandel, Theory of parametric frequency down conversion of light, *Phys. Rev. A* **31**, 2409 (1985).
- [31] O. Gayer, Z. Sacks, E. Galun, and A. Arie, Temperature and wavelength dependent refractive index equations for MgO-doped congruent and stoichiometric LiNbO₃, *Appl. Phys. B* **91**, 343 (2008).